

## Corrected method for scaling the dynamic response of stiffened plate subjected to blast load

Kong, Xiangshao; Zhou, Hu; Kuang, Zheng; Zheng, Cheng; Li, Xiao; Wu, Weiguo; Guan, Zhongwei

**DOI**

[10.1016/j.tws.2020.107214](https://doi.org/10.1016/j.tws.2020.107214)

**Publication date**

2021

**Document Version**

Accepted author manuscript

**Published in**

Thin-Walled Structures

**Citation (APA)**

Kong, X., Zhou, H., Kuang, Z., Zheng, C., Li, X., Wu, W., & Guan, Z. (2021). Corrected method for scaling the dynamic response of stiffened plate subjected to blast load. *Thin-Walled Structures*, 159, Article 107214. <https://doi.org/10.1016/j.tws.2020.107214>

**Important note**

To cite this publication, please use the final published version (if applicable). Please check the document version above.

**Copyright**

Other than for strictly personal use, it is not permitted to download, forward or distribute the text or part of it, without the consent of the author(s) and/or copyright holder(s), unless the work is under an open content license such as Creative Commons.

**Takedown policy**

Please contact us and provide details if you believe this document breaches copyrights. We will remove access to the work immediately and investigate your claim.

1 Corrected method for scaling the dynamic response of stiffened plate  
2 subjected to blast load

3  
4 Xiangshao Kong <sup>a,b</sup>, Hu Zhou <sup>a</sup>, Zheng Kuang <sup>a</sup>, Cheng Zheng <sup>\*a</sup>, Xiao Li <sup>c\*</sup>, Weiguo Wu <sup>a</sup>,  
5 Zhongwei Guan <sup>b</sup>

6 a. Departments of Naval Architecture, Ocean and Structural Engineering, School of  
7 Transportation, Wuhan University of Technology, Wuhan 430063, China.

8 b. School of Engineering, University of Liverpool, Liverpool L69 3GH, UK.

9 c. Department of Maritime and Transport Technology (M&TT), Delft University of Technology,  
10 Netherlands.

11 **Abstract:** Test on a small scaled model is an effective approach to predict the dynamic response of  
12 full scale structure under blast loadings. However, the geometric dimensions of specimens cannot  
13 simply comply with complete geometrical similarity due to manufacture or test restrictions. It would  
14 result in the difference structural performance between the full and small scaled models. This paper  
15 proposed a corrected similarity relationship of the dynamic behaviour between prototype and replica  
16 of stiffened plates subjected to blast load, in which both the thickness of the plate and the  
17 configuration (cross-sectional shape) of stiffeners are distortedly scaled-down (double distorted  
18 geometric scaling factors). Firstly, based on the mesh convergence study and comparing with results  
19 from experimental tests, a numerical method in predicting the confined blast load and dynamic  
20 response of structure was verified, which provides a reliable means to determine the dynamic  
21 behaviour of stiffened plate designed by the corrected similarity criterion of this paper. Then, the  
22 influence of altering the stiffener configuration on the dynamic response of stiffened plates was  
23 analysed and on the basis of it, a criterion for scaling the stiffener is proposed to help design a  
24 stiffener-distorted model from prototype structure. In addition, a method for scaling the double-  
25 parameter distortedly small scaled model is proposed to predict the dynamic response of the  
26 prototype. Finally, two sets of examples of both the small size and prototype stiffened structures

27 subjected to blast load were analysed by using the presented method. It is shown that the replica  
28 developed by applying the present method is able to accurately predict the behaviour of the full-size  
29 stiffened plates, even when the thickness of the plate and the configuration of the stiffeners are  
30 distortedly scaling down with different factors.

31 *Keywords:* corrected similarity relationship, dynamic response, stiffened plate, double geometric  
32 parameters distortion, numerical simulation, confined blast load

## 33 1. Introduction

34 Blast loading produced by an accidental or intentional explosion, such as gas  
35 explosion in inner buildings, missile attack in a combat environment or terrorist attack  
36 on airplanes and public facilities, may provoke not only permanent damage to structures  
37 but also degradation of the environment and human losses <sup>[1, 2]</sup>. Stiffened plates have  
38 been widely used as basic unit in thin-wall structures, such as ship hull and  
39 airplane constructions. A better understanding of the dynamic response of a stiffened  
40 plate subjected to blast loading would help design the structures with enhanced blast  
41 resistance and increase the level of safety for personnel and structures in increasingly  
42 threatening environments. Identifying the best way to investigate the shock response of  
43 these structures under blast loading has always been a challenge task. Researchers and  
44 designers have been of particularly concerning the dynamic responses and damage of  
45 structures under extremely server loading conditions <sup>[3-11]</sup>. It is believed that the full-  
46 scale experiment is the most reliable method of evaluating the anti-blast performance  
47 of structures, but with the huge expenditure and environmental conditions imposed  
48 restrictions on any successive tests. Testing of small scaled models is nowadays still a  
49 valuable design tool, helping researchers to accurately predict the behaviour of  
50 oversized prototypes through scaling laws applied to the experimental results <sup>[5, 12-17]</sup>

51 obtained.

52 However, several limitations and difficulties still persist when applying the  
53 similitude theory through the current methodologies to blast loaded structures. Firstly,  
54 the dynamic response of scaling structures hardly follows the general similarity laws if  
55 they were built with materials that sensitive to strain-rate. Secondly, due to  
56 manufacturing technical restrictions, the configuration of small scaled models cannot  
57 comply with the prototype completely in an overall scaling factor. In that case, some  
58 geometrical parameters of a small scaled model have to be altered to meet the demand  
59 of experiments due to the limitations. The two factors mentioned above would result in  
60 incomplete similarity between the small scaled model and the prototype in practice.  
61 Much work <sup>[18-24]</sup> have been undertaken on the similarity relationship of the dynamic  
62 responses between the incomplete small scaled model structure and the prototype under  
63 impact or blast loads.

64 For the process of structural impact events involves plastic flow and possible local  
65 material fracture<sup>[25]</sup>, the influences of strain-rate strengthening effect on the dynamic  
66 yield stress are remarkable. Therefore, it is still a difficult task in solid mechanics to  
67 establish the strain-stress relationships <sup>[26, 27]</sup>. How to deal with the influence of the  
68 material nonlinearity on the complete similarity remains a major challenge. The  
69 distorted configuration of small scaled models has been posed as the main limitation  
70 for traditional or non-corrected scaling laws in blast or impact scenarios, along with  
71 other limitations such as strain-rate and inertia effects <sup>[16]</sup>. Oshiro and Alves firstly  
72 proposed a Non-Direct Similitude technique <sup>[18, 28, 29]</sup>, which was used to skilfully  
73 address the strain-rate effect on the dynamic yield stress by changing the impact  
74 velocity. This technique provided a reliable and effective method to predict dynamic  
75 responses of a structure subjected to impact or blast loading by using test results of a

76 small size replica. Furthermore, they successfully predicted the dynamic response of  
77 prototypes by using small scaled models that made of different materials or with  
78 distorted configurations [19, 30]. Luo et al. [31, 32] conducted a numerical study on the  
79 scaling of a rotating thin-wall short cylindrical shell. Sensitivity analysis and governing  
80 equations were employed to establish the scaling law between the distorted model and  
81 the prototype, which was aimed to provide an effective scaling law, applicable structure  
82 size intervals and boundary functions that could guide the design of distortion models.  
83 Cho et al. [33] presented the research on the similarity method based on two kinds of  
84 scaled models, one with distorted configurations and the other made of another material.  
85 This study was to overcome the dimensional and material limitations in model tests and  
86 predict the dynamic response of the prototype by combining the two distorted factors  
87 mentioned above. Yao et al. [34] performed an investigation of scaling the deformation  
88 of steel box structures subjected to internal blast loading experimentally and  
89 numerically. In addition, correction of the scaling law for steel box structure was  
90 conducted which considered both the scale-down factor and the scale strain-rate effect.  
91 In our previous work [35], a corrected similarity relationship between the incomplete  
92 small scaled model and the prototype of blast loaded structure was proposed, in which  
93 only one geometric parameter of the model was distortedly scaled.

94 However, another problem arises when more distorted factors needed to be taken into  
95 account in the design of the small scaled model, such as multi-stiffened plates.  
96 Stiffeners on the plate play an important role in energy absorption and blast resistance  
97 of the whole structure. Owing to manufacturing technical restrictions, the distorted  
98 small scaled factors of both the thickness of the plate and the size of stiffeners do not  
99 comply with the overall geometric scaling factors. Also, the configuration of stiffeners  
100 needs to be further altered to meet the requirement of fabrication of experimental

101 sample structures. Here, the configuration change of stiffeners in a small scaled model  
 102 is referred to as the stiffener-distorted model.

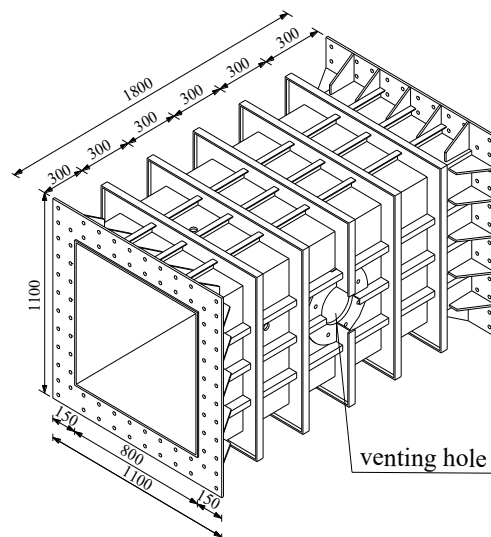
103 A corrected similarity relationship for predicting the dynamic response of stiffened  
 104 plates subjected to blast loads is proposed by using a small scaled model. Here,  
 105 geometric distorted small scaled models are used, in which both the thickness of plates  
 106 and stiffener configurations are distorted. The study includes the development of the  
 107 distortion criterion of stiffener types that is valid when replace the T-type stiffener with  
 108 the flat bar, followed up with a similarity relationship for predicting the dynamic  
 109 response of the prototype. Two analytical examples are introduced to verify the  
 110 reliability of this similarity method by employing a verified numerical method.

<b>Nomenclature</b>		$v$	velocity
		$W$	mass of explosive
<i>Roman symbols</i>		$W_j$	section modulus
		$w$	deflection of the plate
$C$	constant for $C=(\lambda_h)^{n_h}$		
$h$	thickness of the plate	<i>Greek symbols</i>	
$I$	impulse per unit area of shockwave	$\beta$	scaling factor
$I_j$	moment of inertia	$\beta_x$	factor of distorted geometric parameter $x$
$L$	length	$\lambda_x$	factor of distorted geometric parameter $x$
$l_1, l_2$	distance from the centroid of compression and tension area to the neutral axis of the cross-sectional area of stiffener, separately	$\pi$	dimensionless number
$M_0$	plastic limit bending moment	$\rho$	material density
$N_0$	plastic limit neutral plane force	$\sigma_0$	static yield stress
$n_0$	number of stiffeners	$\sigma_d$	dynamic yield stress
$n_l$	exponent		
$R$	stand-off distance	<i>Superscripts</i>	
$S_1, S_2$	static moment from the compression and tension area to the neutral axis of the cross-sectional area of stiffener, separately	$()^m$	small scaled model (reference model)
$S_j$	cross sectional area	$()^p$	prototype
$t$	time	$()^c$	correction model

## 111 2. Numerical simulation method of the blast load and response of structure

112 In order to provide a reliable means to determine the dynamic behaviour of stiffened

113 plate designed by the corrected similarity criterion of this paper, in this section, the  
114 verification of numerical simulation method in predicting the blast load and dynamic  
115 response of stiffened plate was performed. Firstly, mesh convergence studies in  
116 calculating the confined blast load in 2D and 3D space were performed. Then, the  
117 numerical method in predicting the confined blast load and the deflection of stiffened  
118 plates were compared with the measured data from experiments. The schematic  
119 diagram of the experimental device is shown in Fig. 1. It is a hollow cuboid with a  
120 venting hole on one side. The explosive was placed in the middle of this cuboid box  
121 and two specimens of stiffened plates are fixed to the each end of this test device [36].



122

123

Fig. 1. Sketch of the experimental setup (all dimensions in mm)

124

125

126

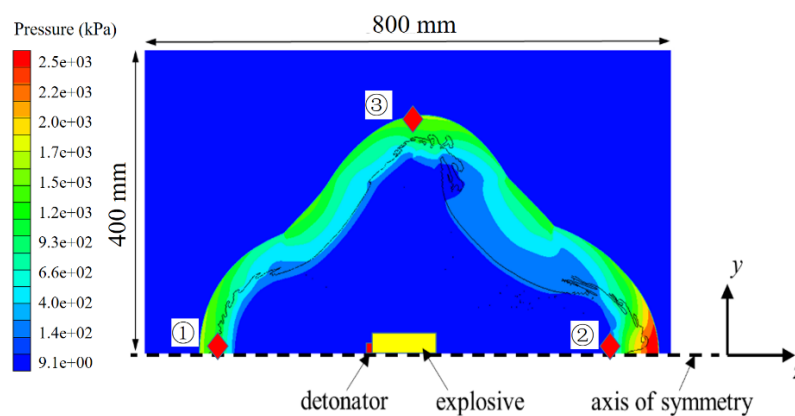
127

128

129

A numerical simulation method was employed to predict the confined blast load and subsequent dynamic response of a stiffened plate by employing ANSYS AUTODYN. In experimental tests, cylindrical explosive charges with different masses and dimensions were used to produce the blast loads. The dimensions of the cylindrical explosive charge are quite smaller than that of the blast test chamber and stiffened plates, so the remapping capability in AUTODYN was employed to reduce the computational cost

130 associated with the initial stages of the calculation which involves the detonation and  
 131 expansion of the cylindrical explosive charge. In order to provide the more accurate  
 132 confined blast loading with relative low computational costs, the pressure field within  
 133 the chamber was produced by mapping in the pressure field resulting from a 2D  
 134 simulation. The region inside the blast chamber, which includes air and explosive  
 135 charge, was firstly modelled using the multi-material Euler formulation in AUTODYN-  
 136 2D, as shown in Fig. 2. The cylindrical TNT enables the 2D axial symmetry condition  
 137 to be used. Due to the mesh size has an influence on the blast load, the mesh sensitive  
 138 studies were firstly performed by discretizing the 2D computational domain with  
 139 different sizes of mesh. Three gauges were placed 100 mm away from the  
 140 corresponding boundary edges to compare the pressure change in conditions of  
 141 different mesh sizes. In this paper, 8 numerical calculations with different mesh sizes  
 142 were performed, in which square grids were used with thickness of 1.33, 1.00, 0.80,  
 143 0.67, 0.57, 0.50, 0.44 and 0.40 mm, respectively.



144 Fig. 2. 2D FE model for blast wave calculation

145 In the numerical simulations, the Jones-Wilkins-Lee (JWL) Equation of State (EOS)  
 146 was implemented to describe the explosive materials, which is defined as,  
 147



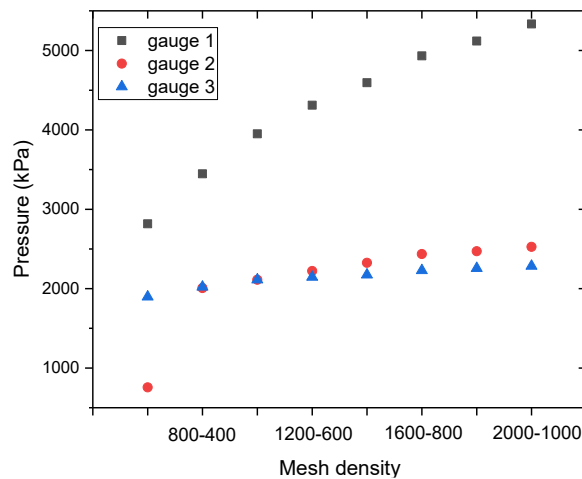
148 
$$p = C_1 \left( 1 - \frac{w}{r_1 v} \right) e^{-r_1 v} + C_2 \left( 1 - \frac{w}{r_2 v} \right) e^{-r_2 v} + \frac{wE}{v} \quad (1)$$

149 In addition, the air is modelled with an ideal gas equation of state as follows,

150 
$$p = (\gamma - 1) \rho e \quad (2)$$

151 where  $\gamma=1.4$  is the heat specific ratio,  $\rho=1.225 \text{ kg/m}^3$  is density,  
 152  $e = 2.068 \times 10^5 \text{ J/kg}$  is internal energy,  $C_1=3.7377 \times 10^5 \text{ MPa}$  ,  $C_2=4.15$  ,  
 153  $r_1=3.75 \times 10^3 \text{ MPa}$  ,  $r_2=0.9$  are constants,  $\omega=0.35$  is the specific heat,  $v$  is  
 154 specific volume.

155 The 2D simulation is terminated before the shockwave reached the nearest edge of  
 156 the computational domain. The peak pressures from the three gauges are collected and  
 157 compared to investigate the influence of mesh size on the calculated shock wave, as  
 158 shown Fig. 3, in which the pressure change represents the comparison of peak pressure  
 159 between the fine mesh and the coarse mesh. It is found that the finer mesh is more  
 160 capable in capturing the peak value of more intensified shock wave, but more time  
 161 consuming. Due to the factor that the size of 2D computation domain is only 400 mm  
 162  $\times$  800 mm, the mesh size of 0.4 mm  $\times$  0.4 mm is adopted in the numerical simulations.



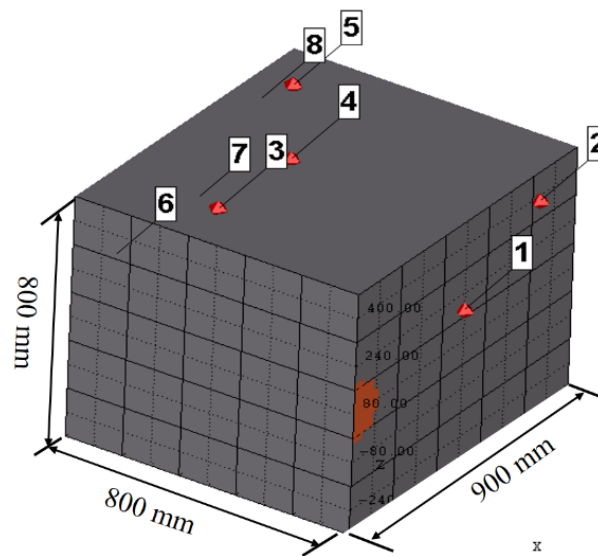
163

164

Fig. 3. Relationship between the mesh density and the peak pressure

165 After the pressure distribution in 2D domain is obtained, it was remapped into 3D  
166 space of the blast chamber, of which the dimensions of length, width and height are  
167 1800 mm, 800 mm and 800 mm, respectively. It is almost impossible to implement the  
168 numerical calculations by employing the same mesh size with that of in 2D  
169 computational domain. In order to find out a suitable model with acceptable accuracy  
170 in predicting the confined blast load, the grid sensitive is also studied for the 3D  
171 computational domain. The symmetry of the problem under consideration allows  
172 modelling only half of the whole inner space of blast chamber, as shown in Fig. 4. The  
173 dimensions of the computational domain are 900 mm, 800 mm and 800 mm, and four  
174 different sizes are used in the conditions of 55 g TNT and 110 g TNT, respectively. In  
175 the numerical calculations, 8 pressure gauges were arranged at different location of the  
176 boundary wall, and the detailed data of gauges 2, 4 and 5 were plotted in Fig. 5(a) and  
177 (b), in which the relationship between the mesh density and peak pressure of the  
178 calculated shock wave in conditions of 55g TNT and 110 g TNT were reflected,  
179 respectively. The comparison shows that when the mesh density was refined from  
180  $90 \times 80 \times 80$  to  $112 \times 100 \times 100$ , the peak pressure was increased by the maximum value of  
181 3.26% and 2.57% among three gauges in conditions of 55 g TNT and 110 g TNT,  
182 respectively. However, the computational cost was increased by 66%. By considering  
183 the balance between efficiency and accuracy, the mesh density of  $90 \times 80 \times 80$  is selected  
184 in the numerical model, resulting in a total number of 576,000 grids. Furthermore, as  
185 the remapping method is employed, the size of the explosive in the 2D domain would  
186 have a slight influence on the calculated blast load in the 3D space. Besides, according  
187 to the Hopkinson scaling law, mass, distance and time can be scaled for explosives over  
188 a wide range of charge sizes <sup>[37]</sup>, so that testing can be conducted at a laboratory scale  
189 and results can be extrapolated to a large scale, reducing the need for full-scale tests.

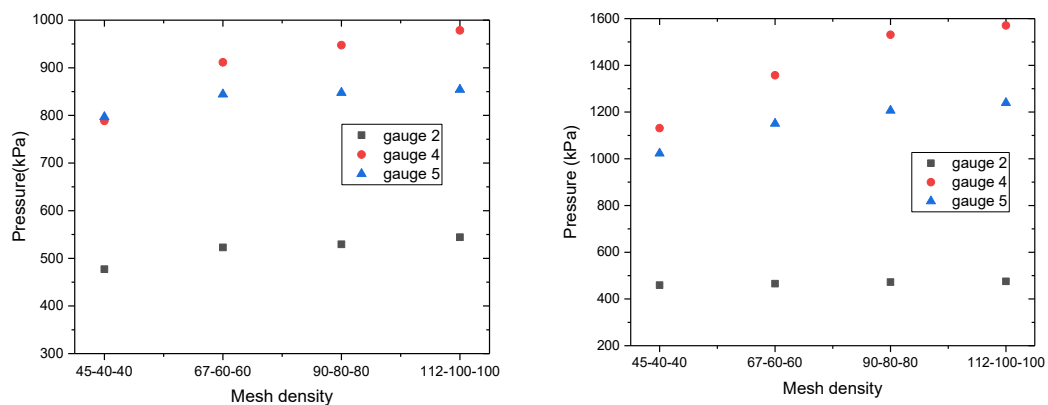
190 The small scaled and prototype of explosions have the same peak value of overpressure,  
 191 and the duration time of shock wave is scaled down with the same factor as the  
 192 geometrical scaling factor. Besides, the responses of stiffened plate under confined blast  
 193 load are usually impulse dependent [38], which is less sensitive to the peak value of  
 194 overpressure of shockwave in confined blast. Thus, in the numerical calculations of  
 195 dynamic responses of stiffened plates subjected to confined blast load, the mesh sizes  
 196 of both the prototype and the small scaled models of 3D computational domain could  
 197 remain unchanged.



198

199

Fig. 4. Three dimensional model and locations of pressure gauges



200

201

(a) 55 g TNT

(b) 110 g TNT

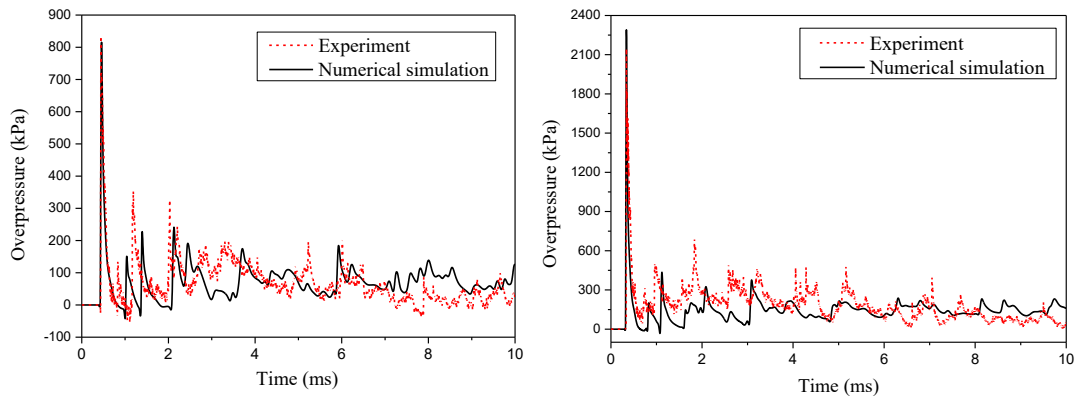
202

Fig. 5. Relationship between the mesh density and peak pressure of calculated shock wave

203

The above verified numerical model is used to calculate the blast load in a partly

204 confined chamber and the results are compared with the measured data from  
205 experiments in Fig. 6. It is shown that the numerical simulation method is capable of  
206 predicting the initial shock wave and rebounded shock wave from walls of chamber,  
207 which would provide a relative accurate input load in the prediction of dynamic  
208 responses of blast loaded stiffened plates.



209

(a) 55 g TNT

(b) 110 g TNT

210

211 Fig. 6. Comparison of pressure-time histories of experiments and numerical simulations

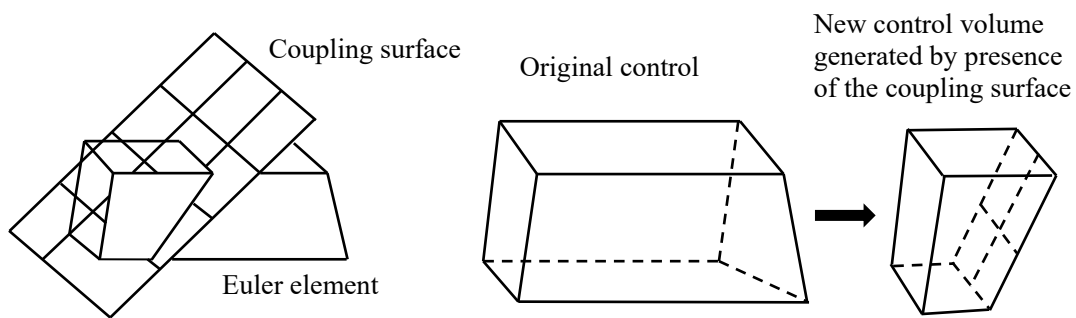
212 Based on the calculation of blast load in confined chamber, the 3D numerical  
213 simulations of the dynamic response of steel plate subjected to confined explosion, in  
214 which the Fluid-Structure Interaction (FSI) process was taken into account to  
215 implement the coupling between the confined blast load and the steel plate, were further  
216 conducted. Generally, structures can be defined in a Lagrangian reference frame where  
217 the mesh follows the material movement, and the Eulerian reference is a more  
218 preferable method to describe the gas flow from detonating explosives. In the present  
219 study, the air is modelled with Euler elements which is an extension of Eulerian  
220 approach, while the steel plates were modelled with Belytschko-Tsay shell elements  
221 based upon Mindlin theory<sup>[39]</sup>. The air domain in the numerical model should be large  
222 enough to cover the deformed plates. Besides, an additional space was provided for the  
223 high pressure air blow out from the venting hole in the wall of experimental setup, as  
224 shown in Fig. 1. Thus, the whole Eulerian domain of air has a dimension of

225 2000×1600×800 mm. The wall including the venting hole is modelled as a rigid  
226 material and meshed with 8 node solid elements. The out-flow boundary conditions are  
227 set on all finite sides of the Euler grid, except on the three specified surfaces, which  
228 represent the rigid walls of the blast chamber, as these are reflective boundaries (no-  
229 flow out condition).

230 A fully coupling algorithm was used to connect the Lagrange solver and Eulerian  
231 solver. As the Lagrange body moves, it acts as a moving boundary in the Euler domain  
232 by progressively covering volumes and faces in the Euler cells. This induces flow of  
233 material in the Euler Domain. At the same time, a stress field will develop in the Euler  
234 domain which results in external forces being applied on the moving Lagrangian body.  
235 These forces will feedback into the motion and deformation (and stress) of the  
236 Lagrangian body. Large deformations may also result in erosion of the elements from  
237 the Lagrangian body. The coupling interfaces are automatically updated in such cases.  
238 In more detail, the Lagrangian body covers regions of the Euler domain. The  
239 intersection between the Lagrangian and Eulerian bodies results in an updated control  
240 volume on which the conservation equation of mass, momentum and energy are solved,  
241 as shown in Fig. 7. In the numerical simulations, the parameter of “cover fraction limit”  
242 in Autodyn is used to determine when a partially covered Euler cell is blended to a  
243 neighbour cell, and the value of cover fraction limit was set to 0.5, which means that  
244 when more than half of the volume is covered, the adjacent Euler domain will be mixed.

245 For obtaining accurate results in the simulation of coupling Lagrangian and Eulerian  
246 bodies in explicit dynamics, it is necessary to ensure that the size of the cells of the  
247 Euler domain are smaller than the minimum distance across the thickness of the  
248 Lagrangian bodies. If this is not the case, the leakage of material in the Euler domain  
249 through the Lagrange structure would occur, resulting in failure of interaction effect. In

250 the case of coupling to thin bodies, of which the thicknesses are small and typically  
251 modelled with shells, an equivalent solid body is generated to enable intersection  
252 calculations to be performed between a Lagrangian volume and the Euler domain. The  
253 thickness of the equivalent solid body is calculated based on the Euler domain cell size  
254 to ensure that at least one Euler element is fully covered over the thickness and no  
255 leakage occurs across the coupling surface. It is noted that the 'artificial' thickness is  
256 only used for volume intersection calculations for the purposes of coupling and is  
257 independent of the physical thickness of the shell/surface body, as shown in Fig. 8. For  
258 the shell solver in Autodyn, the parts do not have any geometric through thickness  
259 dimension, and as such cannot cover any volume in the Euler mesh. Therefore, each  
260 shell part should be artificially thickened. For the coupling methodology to function  
261 correctly, the artificial thickness of a shell must be at least twice the dimension of the  
262 largest cell size in the surrounding Euler grid <sup>[39]</sup>. In the present numerical simulations,  
263 the effective coupling thickness was set to be 25 mm (centred), as the size of the Euler  
264 cell is 10 mm.



265

266

Fig. 7. Schematic diagram of coupling surface and control volume

267

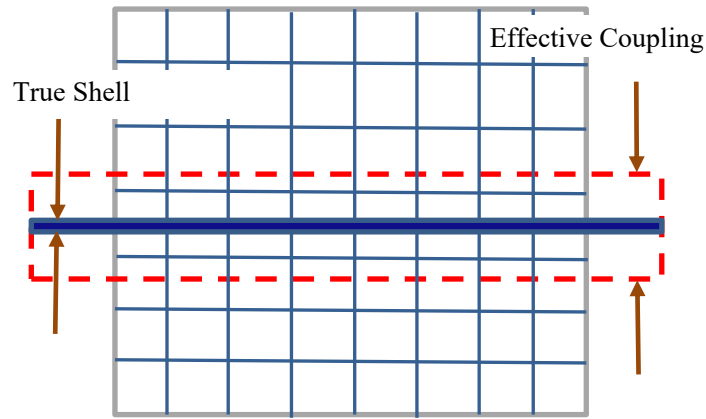


Fig. 8. Schematic diagram of coupling thickness

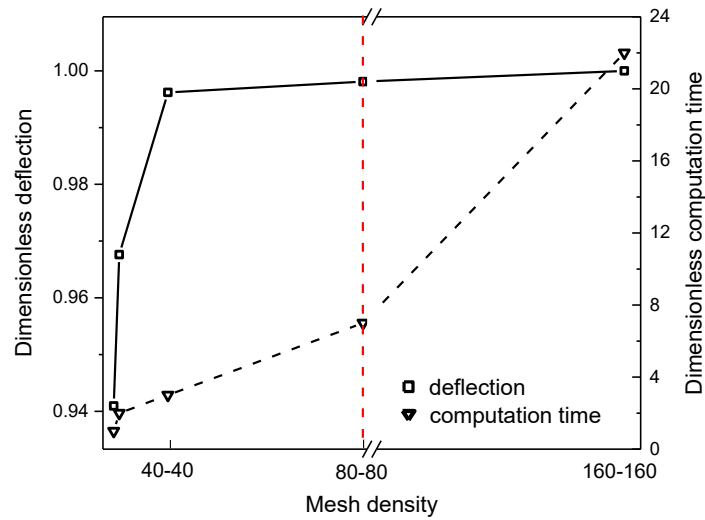
The shell element was used to model steel plate, the material selected from the library of AUTODYN is ‘Piecewise-JC’, which allows the definition of a true stress-strain curve as an offset table. Also, Johnson-Cook strain rate dependency can be defined.

$$\frac{\sigma_d}{\sigma_0} = 1 + C \ln(\dot{\epsilon}) \quad (3)$$

where  $\sigma_d$  is the dynamic flow stress corresponding to the dimensionless plastic strain rate  $\dot{\epsilon}$ ;  $\dot{\epsilon}$  is the effective plastic strain rate;  $\dot{\epsilon}_0$  is the reference strain rate and chosen to be  $1 s^{-1}$ ;  $\sigma_0$  is the associated static plastic flow stress;  $C$  is the empirically determined material constant. This constitutive model is widely used in theoretical and numerical studies on dynamic response of metals under impact and blast loading. For the steel in the present study,  $C = 0.22$ , and static plastic flow stresses of specimens with different thickness are 360 MPa for 1.6 mm, 317 MPa for 2.3 mm and 343 MPa for 3.7 mm specimens respectively.

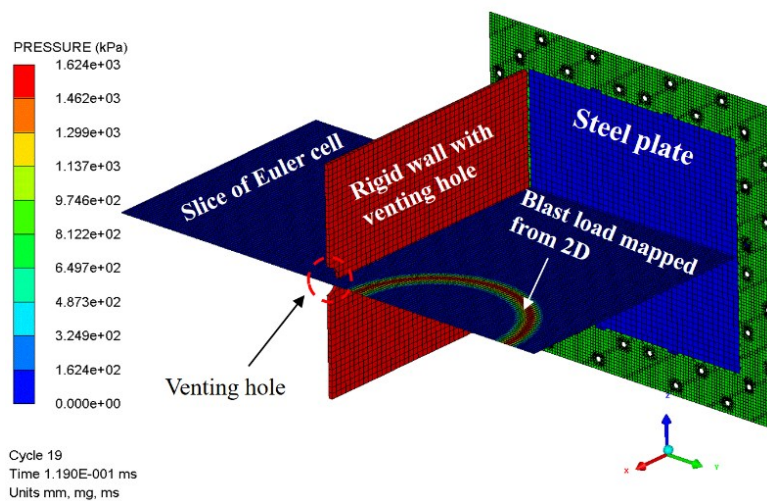
Before the simulations were run on the Euler Lagrangian coupling model, the mesh convergence of steel plate was assessed. The aim is to find the influence of different mesh sizes on the accuracy of residual deflection of blast loaded plate and the computational costs. Five conditions of different mesh density of steel plate, including  $15 \times 15$ ,  $20 \times 20$ ,  $40 \times 40$ ,  $80 \times 80$  and  $160 \times 160$  were calculated, and both the

287 dimensionless deflections (divided by the results from  $160 \times 160$  mesh density  
 288 condition) and dimensionless computation time (divided by the results from  $15 \times 15$   
 289 mesh density condition) were compared, as shown in Fig. 9. In the numerical  
 290 calculations of this paper, the mesh density of  $80 \times 80$  was used guaranteeing a more  
 291 precise reproduction of the dynamic response of steel plate, while keeping the  
 292 computational cost low.



293

294 Fig. 9. Relationship between the mesh density and deflection of blast loaded plate and  
 295 computation time



296

297 Fig. 10. The numerical model of fully Euler-Lagrange coupling calculation (half model)



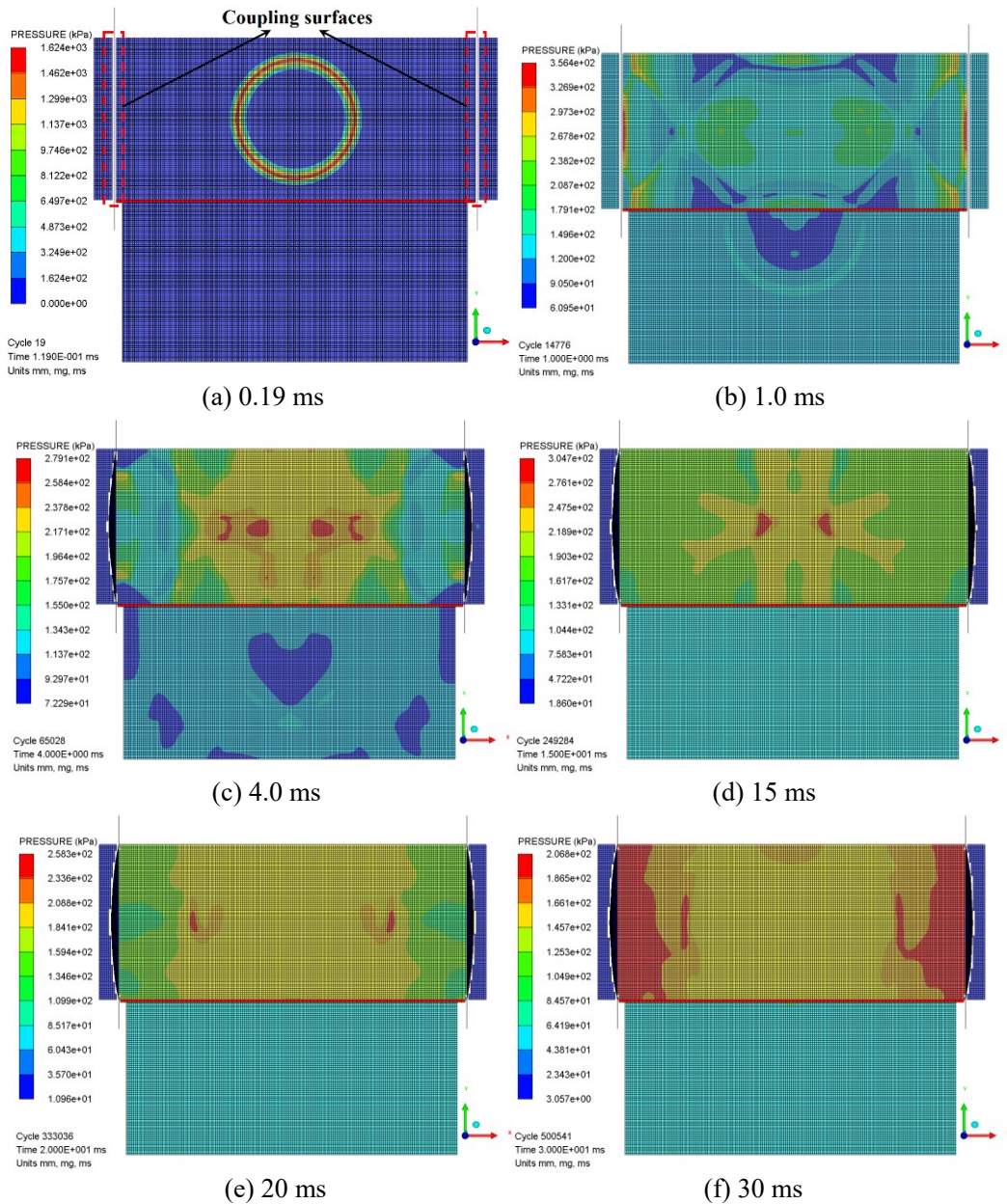


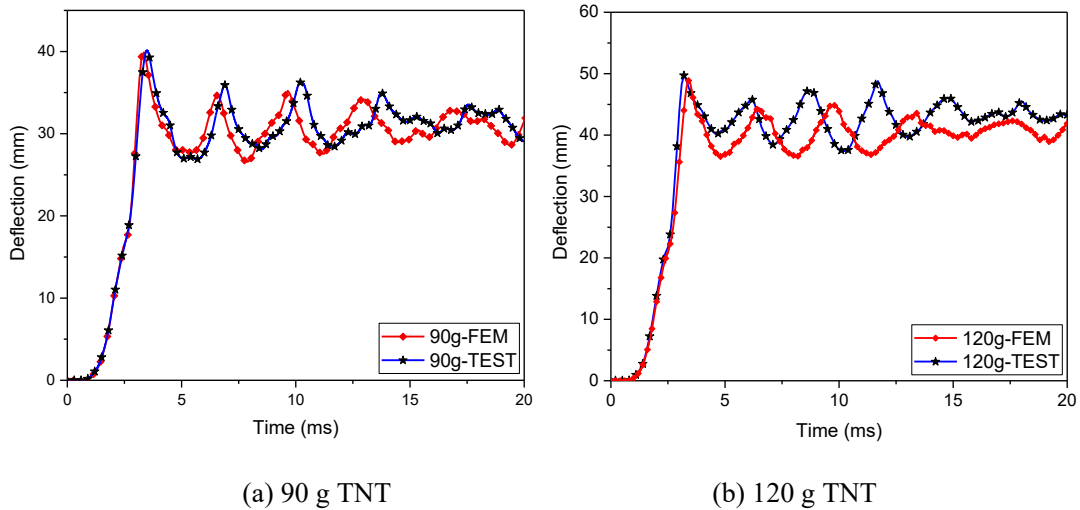
Fig. 11. The movement of coupling surfaces with the deformed steel plates (top view)

Then, the stiffened plates were introduced to the numerical model and the fully Euler-Lagrange coupling is implemented between the steel plates, the wall of blast chamber with venting hole, which was modelled as rigid wall by 8 nodes solid element, and the air inside the confined chamber (just a slice of Euler cell at the horizontal middle cross-section of the whole Euler domain is displayed), as shown in Fig. 10. The blast load was mapped from 2D calculation by using fine mesh. The coupling process of the confined blast pressure and the steel plates with time increasing is shown in Fig. 11.

312 For the sake of clearly showing the interaction effect between Euler cell and Shell/  
313 Lagrangian elements, Fig. 11 is displayed in top view of the whole model in Fig. 10. At  
314 the beginning of the calculation, the 'artificial' thickness attached to the coupling  
315 surfaces was firstly introduced, as shown in Fig. 11 (a). When the steel plates deformed  
316 under the confined blast load, the coupling surface moved accordingly to ensure the  
317 load applied persistently on the deformed plates. Besides, the deformed plates become  
318 updated coupling interfaces and constrained boundary of Euler cells. In the numerical  
319 simulation, no leakage of material in the Euler domain through the steel plate could be  
320 found. However, if erosion of the elements of the Lagrangian structure occurs, the  
321 coupling interfaces would be automatically updated, and the material in Euler cells  
322 would flow through the broken coupling surface.

323 The dynamic response of 4 samples of stiffened plates are predicted by employing  
324 above validated numerical method, and the results of which are compared with  
325 experimental data and summarized in Table 1. The numerical results of residual  
326 deflections of the central point of stiffened plates agree well with the data from  
327 experiments. It is worth noting that the residual deflections in different load conditions  
328 from the numerical simulations are the average value of the oscillation stage after the  
329 first peak deflections, and those values of experiments were measured by employing a  
330 3D laser scanner after explosion when the plates are in steady condition. Besides, the  
331 comparison of the deflection-time histories of a 2.94 mm blast loaded plates (without  
332 stiffeners) between numerical simulations and experiments in the conditions of 90 g  
333 and 120 g TNT are presented in Fig. 12, which revealed that the numerical method  
334 employed in this paper is capable of predicting the dynamic response process of blast  
335 loaded plates with acceptable accuracy. The interaction effect between the blast load  
336 and the structural response in numerical simulations can also be validated. In the

337 numerical simulations of prototype and small scaled models of blast loaded structures,  
 338 the above validated mesh density is recommended. Besides, the numerical model can  
 339 be scaled according to the corresponding geometric scaling factors, but keep the mesh  
 340 density unchanged.



343 Fig. 12. The comparison of deflection-time histories between numerical simulation and  
 344 experimental results

345 Table 1. Results from experimental test and numerical simulations

No.	TNT mass $W$ (g)	Thickness of plates $h$ (mm)	Stiffener $H \times W \times L$ (mm)	Number of stiffeners $n$	Residual deflection of stiffened plates $W$ (mm)	Numerical results (mm)
1	55	1.6	1.6×20×800	2	35.4	35.2
2	55	2.3	2.3×30×800	2	26.3	26.4
3	110	2.3	2.3×30×800	3	43.8	43.7
4	110	3.7	2.7×30×800	3	24.1	24.0

### 346 3. Criteria for altering the stiffener configuration

347 Rolled and built-up T-type stiffened plates are two of the commonly used  
 348 strengthening members in large-scale hull structures. Usually, flat bars are often used  
 349 to replace the T-type stiffeners in small scaled model tests due to manufacturing  
 350 technical restrictions, in which the configurations of stiffeners are different between  
 351 prototype and replica. It is essential to guarantee the flat-bar stiffened model to have

352 the similar dynamic characteristics to its T-type stiffened counterpart. Dimensional  
 353 analysis method is employed to find out the principles that should be followed in  
 354 altering the stiffener type in the small scaled model of a stiffened plate.

355 The dynamic response of the blast loaded steel stiffened plate is related to the  
 356 following parameters, i.e. impulse per unit area of a shockwave  $I$ , length of the plate  $L$ ,  
 357 thickness of the plate  $h$ , material density  $\rho$ , number of stiffeners  $n_0$ , plastic limit  
 358 bending moment  $M_0$  and neutral plane force  $N_0$  of stiffeners, dynamic yield stress of  
 359 material  $\sigma_d$ , cross sectional area of stiffeners  $S_j$ , elastic section modulus  $W_j$  and  
 360 moment of inertia  $I_j$ .

361 If take the midpoint deflection  $w$  of the stiffened plate as the targeted response, then  
 362 there is

$$363 \quad w = f(L, h, \rho, M_0, N_0, n_0, I, \sigma_d, S_j, W_j, I_j) \quad (4)$$

364 A set of fundamental dimensions comprised of dynamic yield stress  $\sigma_d$ , material  
 365 density  $\rho$  and length of the plate  $L$  are selected to give the following dimensionless  $\pi$   
 366 terms.

$$367 \quad \begin{aligned} \pi_1 &= \frac{h}{L}, \pi_2 = \frac{M_0}{\sigma_d L^3}, \pi_3 = \frac{N_0}{\sigma_d L^2}, \pi_4 = n_0, \\ \pi_5 &= \frac{I^2}{\sigma_d \rho L^2}, \pi_6 = \frac{S_j}{L^2}, \pi_7 = \frac{W_j}{L^3}, \pi_8 = \frac{I_j}{L^4} \end{aligned} \quad (5)$$

368 The similarity relationship of the dynamic response between the small scaled model  
 369 and the prototype can be obtained if each term of the models is kept equal to their  
 370 counterparts in the prototype. The geometrical small scaled factor of a stiffened plate is  
 371 expressed as follows

$$372 \quad \beta_L^{mp} = L^m / L^p = \beta \quad (6)$$

373 where  $L^m$  and  $L^p$  are the length of the small scaled model and prototype, respectively;

374  $\beta$  is a scaling factor.

375 The scaled model with complete similarity gives,

$$\begin{aligned} \frac{\pi_1^m}{\pi_1^p} &= \frac{\beta_h^{mp}}{\beta_L^{mp}} = 1, \quad \frac{\pi_2^m}{\pi_2^p} = \frac{M_0^m \sigma_d^p}{M_0^p \sigma_d^m} \left(\frac{L^p}{L^m}\right)^3, \quad \frac{\pi_3^m}{\pi_3^p} = \frac{N_0^m \sigma_d^p}{N_0^p \sigma_d^m} \left(\frac{L^p}{L^m}\right)^2, \quad \frac{\pi_4^m}{\pi_4^p} = \frac{n_0^m}{n_0^p}, \\ \frac{\pi_5^m}{\pi_5^p} &= \left(\frac{I(t)^m}{I(t)^p}\right)^2 \frac{\sigma_d^p \rho^p}{\sigma_d^m \rho^m} \left(\frac{L^p}{L^m}\right)^2 = \frac{(\beta_I^{mp})^2}{\beta_\sigma^{mp} \beta^2}, \quad \frac{\pi_6^m}{\pi_6^p} = \left(\frac{S_j^m}{S_j^p}\right) \left(\frac{L^p}{L^m}\right)^2, \\ \frac{\pi_7^m}{\pi_7^p} &= \left(\frac{W_j^m}{W_j^p}\right) \left(\frac{L^p}{L^m}\right)^3, \quad \frac{\pi_8^m}{\pi_8^p} = \left(\frac{I_j^m}{I_j^p}\right) \left(\frac{L^p}{L^m}\right)^4 \end{aligned} \quad (7)$$

377 Among these  $\pi$  terms,  $\pi_1$ ,  $\pi_4$ ,  $\pi_6$ ,  $\pi_7$  and  $\pi_8$  are independent variables, while the rest  $\pi$   
378 terms are dependent on the material dynamic properties. The incomplete similarity  
379 caused by the strain rate effect was properly corrected by Oshiro and Alves<sup>[18]</sup>. It should  
380 be noted that the values of  $\pi_6 \sim \pi_8$  of scaled model might differ from that of the prototype  
381 if the configuration (cross-sectional shape) of stiffeners on a stiffened plate is changed  
382 due to the restriction of manufacture. Subsequently, other  $\pi$  terms,  $\pi_2$ ,  $\pi_3$  and  $\pi_7$  in  
383 prototype are also unequal to that of the small scaled model. As a result, a dissimilarity  
384 occurs in the dynamic response of the prototype and small scaled model. In order to  
385 satisfy the requirements of predicting the dynamic behaviour of prototype by using the  
386 stiffener-distorted scaled-down models, the terms  $\pi_6$ ,  $\pi_7$  and  $\pi_8$  need to be identical,  
387 which seems impossible. In such the case, therefore, a compromised approach is to keep  
388 one or two  $\pi$  terms same, while the others are as close to their counterparts in the ideal  
389 small scaled model as possible. Thus, three criteria in scaling the stiffener were  
390 considered and compared, i.e.

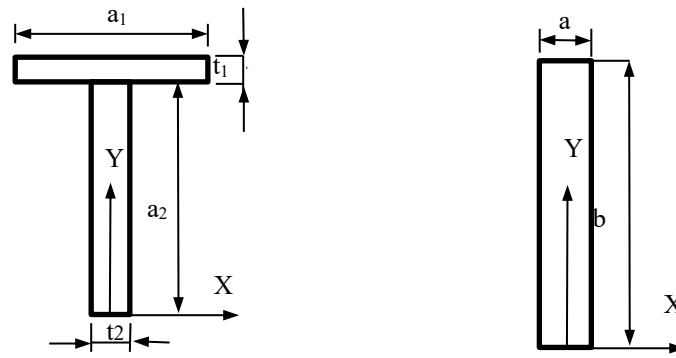
391 Criterion 1, keep the cross sectional area of stiffeners  $S_j$  the same while make the  
392 section modulus  $W_j$  and moment of inertia  $I_j$  to be as close to their counterparts in  
393 the ideal small scaled model as possible.

394 Criterion 2, keep the section modulus  $W_j$  the same while make the cross sectional

395 area of stiffeners  $S_j$  and moment of inertia  $I_j$  to be as close to their counterparts in  
396 the ideal small scaled model as possible.

397 Criterion 3, keep the moment of inertia  $I_j$  the same while make the cross sectional  
398 area of stiffeners  $S_j$  and the section modulus  $W_j$  to be as close to their counterparts  
399 in the ideal small scaled model as possible.

400 Figure 13 shows the cross sectional dimensions and configurations of T-type and I-  
401 type stiffener, respectively.



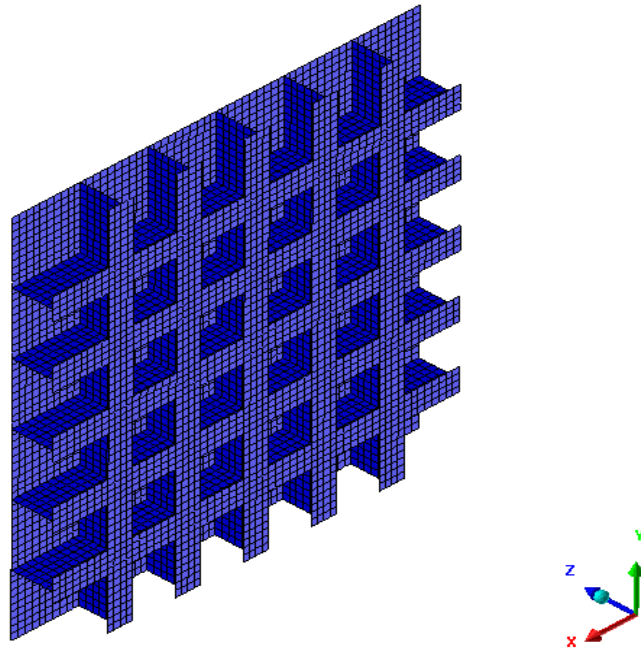
402 (a) T cross-section stiffener

403 (b) I cross-section stiffener

404 Fig. 13. Sketch of cross-sections of stiffeners

405 A square stiffened plate is introduced here to compare the three criteria described  
406 above, as shown in the Fig. 14. The full-scale stiffened plate is 10 meters in length and  
407 10 mm in thickness, with five T cross-section stiffeners (T-type) orthogonally arranged  
408 on the plate. The T-type stiffener has dimensions as  $\perp \frac{1000 \times 8}{600 \times 4}$ , which means the length  
409 and the thickness of flange are 1000 mm and 8 mm, while the corresponding web sizes  
410 are 600 mm and 4 mm, respectively. A blast load was applied on the front side (against  
411 the stiffeners) of the plate from an explosion of 1000 kg TNT in 10 m away from the  
412 centre of the plate. The numerical simulation is conducted by using ANSYS Autodyn,  
413 in which the detailed parameters of numerical model are the same with that presented  
414 by Zhang et al. [40]. The blast load was directly applied on the front face of stiffened

415 plate by defining the boundary as pressure stress of Analytical Blast in Autodyn<sup>[39]</sup>, in  
416 which the propagation of blast wave and its fluid-structure interaction was not taken  
417 into consideration in free air explosion. The calculated residual deflection at its centre  
418 point of this prototype is 188 mm.



419  
420

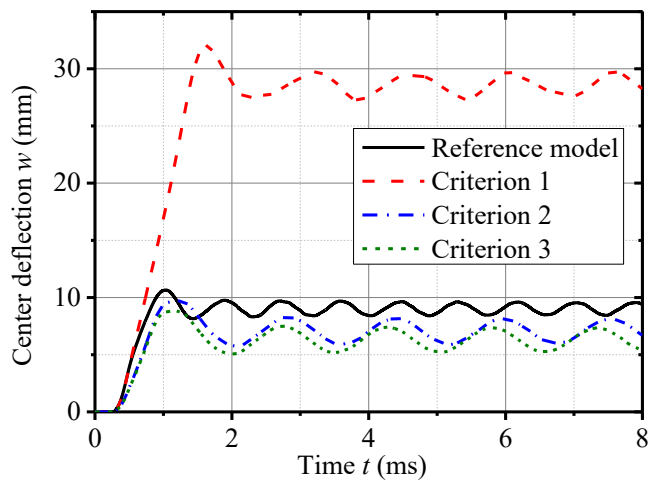
Fig. 14. Schematic diagram of the numerical model of the stiffened panel

421 Assuming stiffeners' thickness of small scaled models not to be less than 2 mm, then  
422 three kinds of different cross sectional dimensions of the I-shaped stiffeners for the  
423 distorted models can be designed according to the above three criteria, which are listed  
424 in Table 2. For comparison, a reference model, with both the thickness and  
425 configuration of stiffeners being ideally scaled down by a factor of 1:20 from its  
426 prototype, is also built to analyse its dynamic behaviour. In this paper, the 1:20 scaling  
427 problem was solved by employing equations and numerical simulation to illustrate the  
428 application process of the present method. Actually, any other scaling factor can be used.  
429 However, an appropriate scaling factor between prototype and small scaled model  
430 should be determined due to some restrictions in practice. It should be noted that the  
431 numerical model of the small scaled structure has the same amount of grids with the

432 prototype model.

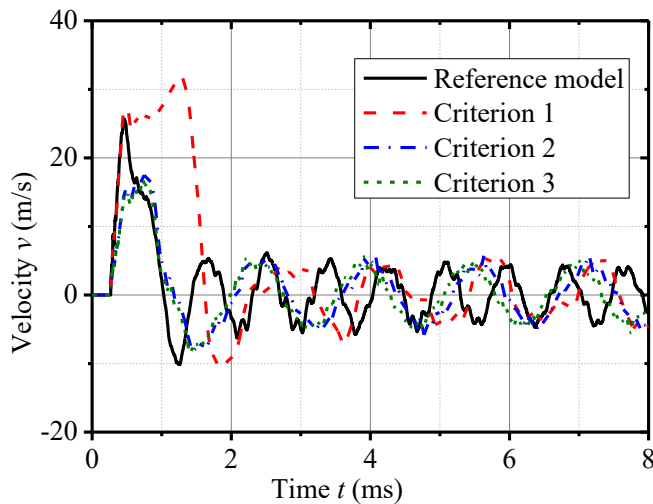
433 Table 2. Cross sectional parameters of the small scaled stiffeners

Criterion No.	Reference model (stiffeners are ideally scaled down )	1	2	3
Cross sectional dimension (mm)	$\pm \frac{50 \times 0.4}{30 \times 0.5}$	18×2	41×2	43×2
Cross sectional area $S_j$ (mm <sup>2</sup> )	35	36	82	86
Section modulus $W_j$ (mm <sup>3</sup> )	1080	216	1121	1233
moment of inertia $I_j$ (mm <sup>4</sup> )	54542	3888	45947	53005
TNT mass $W$ (kg)	0.125	0.125	0.125	0.125
Stand-off distance $R$ (mm)	500	500	500	500



434

435 Fig. 15. Comparison of the deflection-time curves among the three criteria



436

437

Fig. 16. Comparison of the velocity-time curves among the three criteria

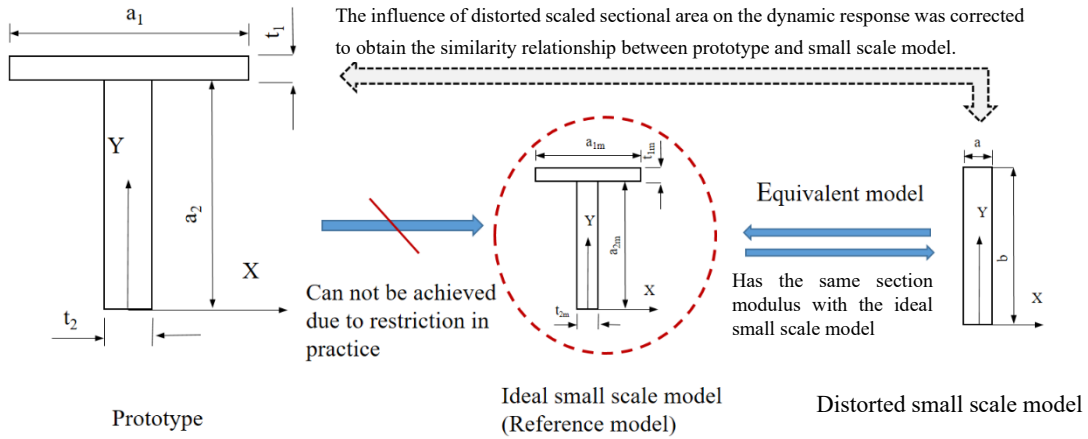


438       Selecting the dynamic response of the plates at the centre point of the stiffened plate  
439 as an object, the comparison results of deflection and velocity-time curves for each  
440 small scaled model in complying with the related three criteria are shown in Fig. 15 and  
441 Fig. 16. The comparative results show that the plate designed conforming to Criterion  
442 2 has the most similar behaviour with the ideal reference model no matter in  
443 displacement or velocity under blast loads. This indicates that the stiffeners may have  
444 reasonably approximate dynamic behaviour when keep the section modulus the same  
445 while make the other two terms to be as close to their counterparts as possible. Based  
446 on the analysis above, Criterion 2 for stiffeners will be employed in the following  
447 analysis. The small scaled model designed by employing the Criterion 1, which had the  
448 same cross section area with the reference model, experienced much larger deflection.  
449 It means that it is the absorption of the bending energy but not the inertial effect of the  
450 stiffeners mainly affected the dynamic behaviour of the blast loaded stiffened plates.

451       Although Criterion 2 ensures the stiffened plate with distorted stiffener having the  
452 most similar dynamic behaviour to its prototype, it should be noted that the dynamic  
453 response of the stiffener distorted model still has deviations from that of the reference  
454 model. It needs further corrections before it can be used to predict the dynamic response  
455 of its prototype, in which the schematic diagram for altering the configuration of  
456 stiffener is shown in Fig.17. A distorted geometric parameter of the stiffener could be  
457 taken into account to help building a more accurate similarity relation between the  
458 stiffener distorted small scaled mode and the prototype.

459       Considering the overall deflection of the stiffened plate to be closely related to its  
460 energy absorption, the energy absorption of stiffeners (as a part of the stiffened plate)  
461 will be affected by their plastic limit bending moment  $M_0$  and neutral plane force  $N_0$ .  
462 The cross sectional area  $S_j$  of the stiffeners may be selected as the geometrical

463 correction parameter.



465 Fig. 17. The schematic diagram for altering the configuration of stiffener

466 The plastic limit bending moment  $M_0$  of stiffeners can be obtained from the following

467 formula,

$$468 \quad M_0 = \sigma_d (S_1 + S_2) = 0.5 \sigma_d S_j (l_1 + l_2) \quad (8)$$

469 The neutral plane force  $N_0$  of stiffeners corresponding to plastic limit is,

$$470 \quad N_0 = \sigma_d S_j \quad (9)$$

471 where  $S_1$  and  $S_2$  are the static moments from the compression and tension areas to  
 472 the neutral axis of the cross-sectional area of the stiffener, respectively;  $l_1$  and  $l_2$   
 473 represent the distance from the centroid of the compression and tension area to the  
 474 neutral axis of the cross-sectional area of the stiffener, respectively.

475 A geometrical distortion factor about the cross sectional area  $S_j$  of the stiffener is  
 476 defined as follows,

$$477 \quad \beta_{S_j} = (S_j)^d / (S_j)^p \quad (10)$$

478 where  $(S_j)^d$  and  $(S_j)^p$  represent the cross sectional areas of distorted small scaled  
 479 stiffener and prototype stiffener, respectively.

480 Besides, a corresponding distortion coefficient of the cross sectional area is defined

481 below,

482 
$$\lambda_{S_j} = (S_j)^d / (S_j)^m = \beta_{S_j} / \beta \quad (11)$$

483 Thus a correction equation for the impulse per unit area of the shockwave  $I^c$  is  
484 given by

485 
$$I^c = I^m \lambda_I = I^m \lambda_{S_j}^{n_I} \quad (12)$$

486 where  $I^m$  and  $I^c$  are the impulse per unit area applied on the reference model and  
487 the distorted model, respectively.  $n_I$  is an exponent related to the distorted  
488 geometrical parameters and the impulse per unit area.

489 The corrected TNT mass for the distorted model can be determined based on the  
490 result of Eq. (12), of which the flow chart is shown in Fig. 18. Firstly, a pair of small  
491 scaled models with different distortion scaling factors of the cross section, Model A and  
492 Model B were designed and introduced. The detailed parameters of the three different  
493 models of the stiffener plates are listed in Table 3, in which the reference model is the  
494 ideally scaled model with no distortion parameters.

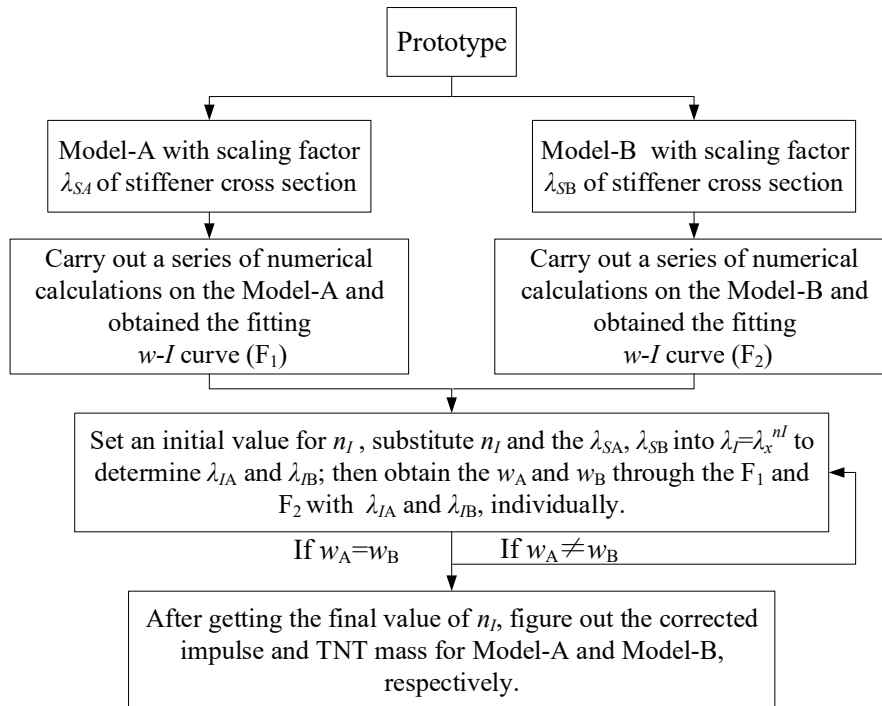


Fig. 18. The flow chart of the method for determining the corrected TNT mass

495

Table 3. Relevant parameters of the two stiffener-distorted models

Name	Stiffener (mm)	Cross section $S_j$ (mm <sup>2</sup> )	Section modulus $W_j$ (mm <sup>3</sup> )	Moment of inertia $I_j$ (mm <sup>4</sup> )	Distortion coefficient of the cross section $\lambda_{Sj}$
Reference model	$\perp \frac{50 \times 0.4}{30 \times 0.5}$	35	1080	54543	1.00
Model-A	41×2	82	1121	45947	2.34
Model-B	36×2.5	90	1080	38880	2.57

496

By employing the verified numerical method presented in Section 1, a series of numerical calculations with different loading conditions of TNT mass were performed to predict the dynamic response of the three small scaled models, as listed in Table 4.

497

498

499

Table 4. The computing results of each distorted model

No.	Model-A1	Model-A2	Model-A3	Model-A4	Model-A5	Model-A6
TNT mass (g)	130	135	140	145	150	155
$I$ (Pa·s/m <sup>2</sup> )	365.07	373.29	381.38	389.35	397.20	404.93
$w$ (mm)	7.39	7.86	8.32	8.75	9.20	9.61
No.	Model-B1	Model-B2	Model-B3	Model-B4	Model-B5	Model-B6
TNT mass (g)	170	175	180	185	190	195
$I$ (Pa·s/m <sup>2</sup> )	427.49	434.81	442.04	449.17	456.22	463.18
$w$ (mm)	1045	10.82	11.26	12.65	12.01	12.38

500

A set of data of the centre point deflection ( $w$ ) and the impulse per unit area ( $I$ ) for each model are collected, and their relationship ( $I$ - $w$  curve) can be determined subsequently by data fitting. Thus two  $I$ - $w$  relationships  $F_1$  and  $F_2$  for Model-A and Model-B can be established, which are given as

501

502

503

504

$$F_1 : w_A = 0.0555I_A - 12.863 \quad (13)$$

505

$$F_2 : w_B = 0.0533I_B - 12.308 \quad (14)$$

506

The fitting relationship for TNT mass and impulse per unit area ( $W$ - $I$  curve) from the numerical simulations is given as

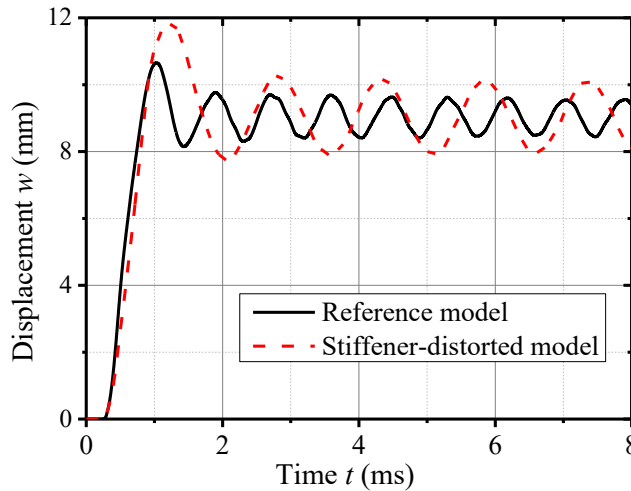
507

508 
$$W = 0.6321I - 101.02 \quad (15)$$

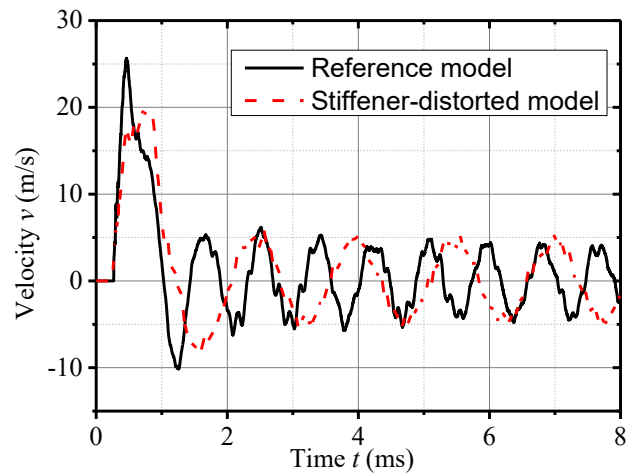
509 For example, when the load from the explosion of 125 g TNT was applied to the  
 510 reference model, as listed in Table 3, the value of the impulse per unit area  $I^m$  applied  
 511 on the stiffened plate was calculated by Eq. (15),  $I^m = 357 \text{ Pa}\cdot\text{s}$ . The correction  
 512 exponent  $n_l$  can be solved by taking  $I^m$ ,  $F_1$  and  $F_2$  into the computing programs,  
 513 with its value determined as 0.112. Thus the corrected impulse per unit area for Model-  
 514 A is

515 
$$I_A^c = I^m \lambda_{SA}^{n_l} = 357 \times 2.34^{0.112} = 392 \text{ Pa}\cdot\text{s} \quad (16)$$

516 The corresponding corrected TNT mass for Model-A is 147 g, which can be acquired  
 517 by inserting the value of  $I_A^c$  in Eq. (15). By applying the corrected TNT mass to the  
 518 Model-A (here the Model-A is employed to predict the dynamic response of the  
 519 prototype), a value of 8.91 mm in residual centre deflection of the stiffened plate is  
 520 obtained, which is very close to that of the reference model (8.92mm). Here, the  
 521 residual centre deflection of the model is the average value of crest and trough in the  
 522 oscillation stage of the curve. The comparison of deflection- and velocity-time  
 523 predictive curves between the reference model and Model-A with the corrected TNT  
 524 mass are shown in Fig. 19 and Fig. 20, respectively.



526 Fig. 19. Comparison of the displacement-time histories between the stiffeners distorted model and  
527 the reference model



528  
529 Fig. 20. Comparison of the velocity-time histories between the stiffeners distorted model and the  
530 reference model

531 As indicated in Fig. 18, the difference of residual centre deflection between the  
532 corrected model and the reference model is relatively small, though there is a deviation  
533 in their maximum displacement. Although the predicted maximum velocity (Fig. 20) is  
534 not as good as the deflection in comparison to that of the reference model, the overall  
535 velocity-time history curve predicted has better correlation than the results in Fig. 16.  
536 These comparison results indicate that the influence of the change of the cross sectional  
537 area  $S_j$  of the small scaled model on the similarity of the dynamic behaviour between  
538 replica and prototype can be effectively corrected by using the updated TNT mass.

#### 539 4. Scaled models considering double geometric parameters

540 In this section a more complex situation of the distorted small scaled model in both  
541 stiffener types and thickness of the plate will be further studied based on the corrected  
542 method for stiffener distorted model presented in Section 3.

543 For the models distorted in both stiffener configuration and thickness of plates, the  
544 correction equation Eq. (12) used in the stiffener distorted model can be developed  
545 into the following form

546 
$$I^c = I^m (\lambda_h)^{n_{I1}} (\lambda_{Sj})^{n_{I2}} \quad (17)$$

547 where  $n_{I1}$  and  $n_{I2}$  are two exponents related to the distorted scaling thickness of  
 548 plates and the cross sectional area of stiffeners, respectively.

549 The difficulty in using Eq. (17) to obtain a correct factor of  $I^c$  is how to determine  
 550 the value of the first coefficient  $n_{I1}$  for a scaled model considering double geometric  
 551 parameters double geometric parameter distorted model and thus pose a barrier to solve  
 552 the second unknown exponent  $n_{I2}$  with the method proposed in our previous research  
 553 work [35].

554 In order to solve the exponents in Eq. (17), it is necessary to simplify this equation.  
 555 Considering the exponent  $n_x$  has a fixed value in a specific distorted model, if the  
 556 thickness of the plate of this model is distorted with a fixed distortion coefficient  $\lambda_h$ ,  
 557 then the item  $(\lambda_h)^{n_{I1}}$  in Eq. (17) can be replaced with an unknown constant  $C$  and thus

558 
$$I^c = I^m C (\lambda_{Sj})^{n_{I2}} \quad (18)$$

559 Here, the simplified Eq. (18) can be solved according to the following steps.  
 560 Step 1: establish three distorted models Model-A, Model-B and Model-C with identical  
 561 size, which have the same plate thickness to ensure the same thickness distortion  
 562 coefficients  $\lambda_h$  but with different cross sectional area and stiffeners distortion  
 563 coefficients, i.e.  $\lambda_{SA}$ ,  $\lambda_{SB}$  and  $\lambda_{SC}$ . It should be noted that the distorted small scaled  
 564 model in cross sectional area of stiffeners should follow Criterion 2 given in Section 2.  
 565 Then a series of TNT mass selected from a narrow range deviated from the TNT mass  
 566  $W^m$  of the small scaled reference model (without distortion) are applied to the distorted  
 567 models to calculate the dynamic response numerically.  
 568 Step 2: take one parameter of dynamic response as the object of study, for instance, the





Prototype	1.0	10000	10	1.0	$\pm \frac{1000 \times 8}{600 \times 10}$	14000	1.0
Scale-down reference model	0.05	500	0.5	1.0	$\pm \frac{50 \times 0.4}{30 \times 0.5}$	35	1.0
Model-A	0.05	500	1.0	2.0	41×2.0	82	2.34
Model-B	0.05	500	1.0	2.0	36×2.5	90	2.57
Model-C	0.05	500	1.0	2.0	47×1.5	70.5	2.01

588 A series of TNT mass  $W$  of 190, 195, 200, 205 and 210 g are selected and the values  
589 of their corresponding impulse per unit area of the shockwave  $I$  applied on the stiffened  
590 plate are computed. The  $W$ - $I$  fitting formula is given as follows,

$$591 \quad W = 0.7314I - 143.73 \quad (20)$$

592 By applying the above TNT masses selected to the distorted models, the final  
593 deflection at the centre point of blast loaded stiffened plates can be obtained. Then a set  
594 of  $w$ - $I$  formulas can be fitted and given as follows,

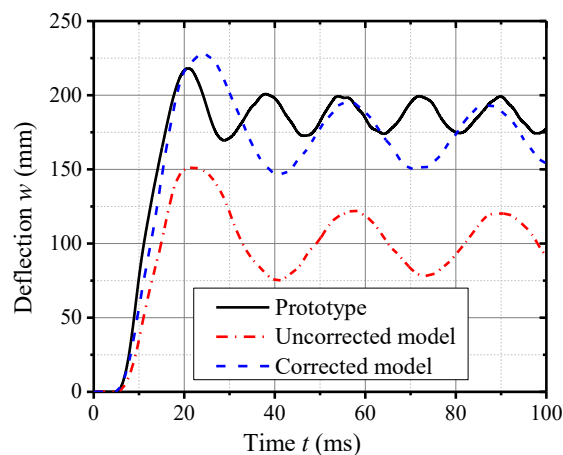
$$595 \quad \begin{aligned} \text{Model-A, } F_A : w_A &= 0.0445I_A - 10.998 \\ \text{Model-B, } F_B : w_B &= 0.0432I_B - 10.811 \\ \text{Model-C, } F_C : w_C &= 0.0549I_C - 14.804 \end{aligned} \quad (21)$$

596 For the 1:20 ideal small scaled reference model, its TNT mass  $W^m$  is 127.5 g after  
597 taking the scaling factor and strain-rate effect into account and the value of the  
598 corresponding impulse per unit area  $I_0$  of the adjusted TNT mass is 359 Pa·s .  
599 Substituting the  $I_0$  determined into Eq.(19), the values of  $C$  and  $n_{I_2}$  are obtained as  
600 below.

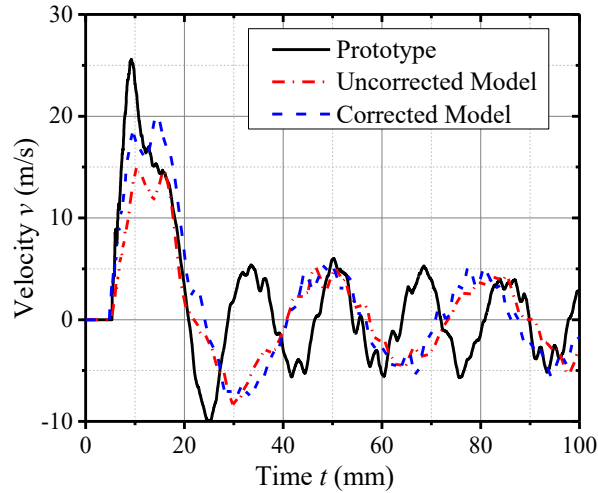
$$601 \quad C = 1.02, \quad n_{I_2} = 0.216 \quad (22)$$

602 The corrected impulse  $I_A^c$  of Model-A stiffener plate at the centre point is  
603  $I_A^c = 440.1 \text{ Pa} \cdot \text{s}$  and finally, the corrected TNT mass  $W_A^c$  for Model-A is obtained  
604 by Eq. (20) as 178.2 g.

605 By applying the updated TNT mass to Model-A, the residual deflection 8.60 mm of  
606 the stiffener plate at its centre point can be obtained through numerical calculations.  
607 Based on the result of Model-A, the corresponding value of the residual deflection of  
608 the prototype predicted is 172 mm, which is very close to the value of 188 mm  
609 calculated directly from the full-size structure. Fig. 21 and Fig. 22 show the comparison  
610 of the predicted displacement- and velocity-time history curves from the uncorrected  
611 model, the corrected distorted model and the prototype, respectively. It is found that the  
612 present corrected method provides a better prediction of the dynamic behaviour of the  
613 full-size structure, reducing the deviation from 47 % to 8.48 %, as shown in Fig. 21. It  
614 is worth noting that the TNT mass for the uncorrected model was determined according  
615 to the geometrical scaling factor, which is approximately equal to the cube root of the  
616 TNT mass for the prototype. That is to say, the influence of the distortion scaling factors  
617 on the dynamic response was not considered for the uncorrected model, resulting in  
618 much lower predicted deflection than that of the corrected model when subjected to  
619 blast load. Although the predicted velocity shows some discrepancy, the corrected  
620 model still gives better predicted results of the maximum velocity for the prototype, as  
621 shown in Fig. 22.



622  
623 Fig. 21. Comparison of the deflection-time histories between prototype, uncorrected and corrected  
624 models



625

626 Fig. 22. Comparison of the velocity-time histories between prototype, uncorrected and corrected  
627 models

628 5.2 The dynamic behaviour of a stiffened plate subjected to confined blast load

629 Take the four stiffened plates listed in Table 1 as prototypes, three distorted small  
630 scaled models with double geometric parameters for each prototype were designed to  
631 determine the value of  $C$  and  $n_{12}$  by employing the method presented in Section 4.  
632 The relevant geometric parameters of each distorted small scaled model are given in  
633 Table 6.

634 Here taking Case No.1 as an example to predict its dynamic behaviour under  
635 confined blast load by using three 1:10 small scaled models, both the geometric  
636 parameter of plate thickness and the size of stiffener are distorted small scaled with  
637 different factors. It is noted that the design of distorted stiffeners follows Criterion 2  
638 presented in Section 2, which keeps the section modulus  $W_j$  unchanged, while the  
639 cross sectional area of stiffeners  $S_j$  and moment of inertia  $I_j$  are as close to their  
640 counterparts of the ideal small scaled model as possible. The detailed parameters of the  
641 scaled stiffener in Case No.1 are listed in Table 7.

642 Table 6. Geometric parameters and scaling factor of each distorted small scaled model

No.	Scaling factor $\beta$	Distortion coefficient of the thickness of plates $\lambda_h$	Cross sectional area of stiffeners (mm)		
			Model-A	Model-B	Model-C
1	0.1	2	1.8×0.2	1.6×0.25	1.5×0.3
2	0.1	2	2.9×0.25	2.6×0.3	2.4×0.35
3	0.1	2	2.9×0.25	2.6×0.3	2.4×0.35
4	0.1	2	2.8×0.3	2.6×0.35	2.5×0.4

643

Table 7. Parameters of the stiffeners in Case No.1

Case No.1	Scaling factor $\beta$	Stiffener (mm)	Cross sectional area $S_j$ (mm <sup>2</sup> )	Section modulus $W_j$ (mm <sup>3</sup> )	Moment of inertia $I_j$ (mm <sup>4</sup> )	Distortion coefficient of cross section area $\lambda_{sj}$
Prototype	1	20×1.60	32	213	4267	1.000
Model-A	0.1	1.8×0.20	0.36	0.216	0.3888	1.125
Model-B	0.1	1.6×0.25	0.40	0.213	0.3413	1.250
Model-C	0.1	1.5×0.3	0.45	0.225	0.3375	1.406

644

645 A series of TNT masses, which are close to the mass ideally scaled down by using  
646 the overall scaling factor are applied to Model-A, Model-B and Model-C and the  
647 corresponding residual deflection at the centre point of the stiffeners plates are collected.  
648 The validated numerical method was employed to conduct the dynamic responses of  
649 different models under the confined blast load from different masses of TNT. With the  
650 data collected three sets of the  $w-I$  equation for each model are obtained, which are  
651 given as follows,

$$\begin{aligned}
\text{Model-A, } F_A: w_A &= 0.2364I_A + 0.2945 \\
\text{Model-B, } F_B: w_B &= 0.2186I_B + 0.5255 \\
\text{Model-C, } F_C: w_C &= 0.2661I_C - 0.1944
\end{aligned} \tag{23}$$

653 and so as the  $W-I$  relation,

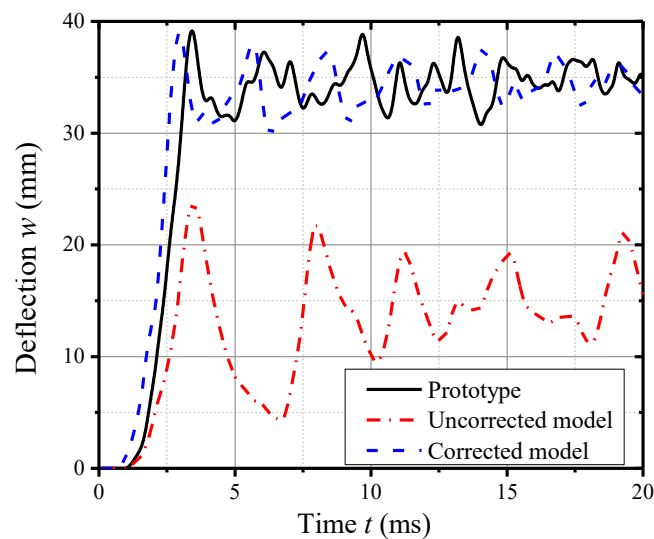
$$W = 1.044 \times 10^{-2} I - 9.524 \times 10^{-3} \tag{24}$$

655 The TNT mass  $W$  for the prototype is 55 g, thus the TNT mass  $W^m$  applied to the  
656 1:10 ideal small scaled model (without geometric distortion) needs to be determined.  
657 The corresponding impulse per unit area  $I^m$  at the centre point of the ideal small scaled  
658 stiffener plate is 6.054 Pa·s. Solving Eq. (23) with the above parameters, the values of

659  $C$  and  $n_{I_2}$  are obtained.

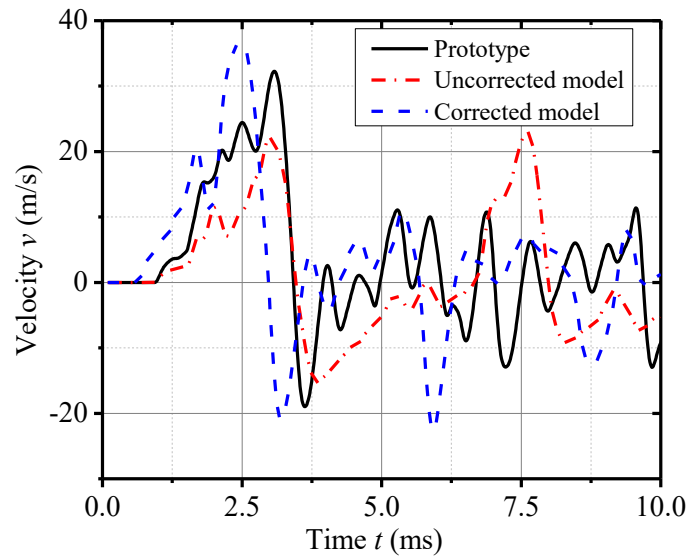
660 
$$C = 2.349, n_{I_2} = 0.073 \quad (25)$$

661 Then, the corrected value of the impulse per unit area  $I_A^c$  for Model-A is 14.343  
662 Pa·s and a corrected TNT mass is determined from Eq. (24). The updated TNT mass  
663 is then applied in the numerical simulations by the distorted small scaled model. The  
664 comparison of the displacement- and velocity-time history curves of the prototype, the  
665 predicted value from uncorrected and corrected models are shown in Fig. 23 and Fig.  
666 24, respectively. It is found that a good agreement is achieved, of which the value of  
667 residual deflection of the prototype stiffened plate predicted by the corrected Model-A  
668 is 36.9 mm, while that from the experimental test and numerical simulation of the full  
669 size stiffened plate given in Table 1 are 35.4 mm and 35.2 mm. The errors on the  
670 predicted residual deflections are 4.02 % and 4.63 %, respectively. It is obvious that the  
671 predicted deflection by using uncorrected model is much lower than that of the  
672 prototype and corrected model, for the uncorrected TNT mass was employed in the  
673 numerical simulations, while the TNT mass applied to the corrected model was properly  
674 altered according to the double distortion scaling factors of the stiffened plate by  
675 employing the method presented in this paper.



676

Fig. 23. Predicted deflection-time curves of the uncorrected and corrected models



678

679

Fig. 24. Predicted velocity-time curves of the uncorrected and corrected models

680

The dynamic responses predicted for rest of the cases with the same correction

681

method are listed in Table 8. Clearly, the corrected method proposed in this paper is

682

capable of determining the dynamic behaviour of the full size stiffened plate by using

683

the double geometric distortedly small scaled model with an acceptable accuracy.

684

Table 8. Predicted results of the double-parameter distorted model in each case

Case No.	1	2	3	4
TNT mass $W$ (g)	0.055	0.055	0.011	0.011
Stand-off distance $R$ (mm)	90	90	90	90
Scaling factor $\beta$	0.1	0.1	0.1	0.1
Distortion coefficient of the thickness of plates $\lambda_h$	2.0	2.0	2.0	2.0
Stiffener of the small scaled distorted model (mm)	1.8×0.2	2.9×0.25	2.9×0.25	2.8×0.3
Constant $C$	2.349	2.973	2.257	2.695
Correction exponent $n_f$	0.073	0.037	-0.014	0.010
Corrected impulse per unit area $I$ (Pa·s)	14.343	18.03	25.78	30.843
Corrected TNT mass $W$ (g)	0.140	0.178	0.262	0.316
Numerical results of the center deflection $w^c$ (mm)	3.465	2.800	4.512	2.421
Prediction result $w^p$ (mm)	34.65	28.00	45.12	24.21

685

## 686 6. Conclusions

687 A verified numerical method in calculating the confined blast load and dynamic  
688 response of stiffened plate was presented. By employing remapping technique, the  
689 pressure distribution of blast load in a 2D domain could be mapped into a 3D domain  
690 with higher accuracy comparing to that directly obtained from the 3D calculation. The  
691 predicted results from the numerical method presented in this paper agree well with the  
692 experimental data both in confined blast and deflection of stiffened plate. Based on the  
693 Hopkinson scaling law, the numerical method can be further employed to predict the  
694 blast load and dynamic response of small scaled model and prototype of structures,  
695 which provides a reliable means to verify the proposed similarity method.

696 A corrected scaling method for predicting the dynamic behaviour of the prototype of  
697 stiffened plates under blast loads by using its distortedly small scaled model with  
698 double-geometric parameters has been proposed and verified in this paper. The  
699 situations of both the thickness of the plate and the type of stiffeners are distortedly  
700 small scaled with different factors are considered. Unlike the single-geometric  
701 parameter distorted case, the double-geometric parameters distortedly small scaled  
702 model has to be more carefully designed and the distortion of their stiffeners should  
703 conform to Criterion 2 outlined in Section 3. It is worth noting that the section modulus  
704 of the stiffener should be given priority to distorting the stiffener configuration, the  
705 cross sectional area and the moment of inertia of the stiffener, as close to that of the  
706 ideal small scaled model as possible. This is the key point to keep the stiffener  
707 distortedly small scaled model having the most similar dynamic behaviour to its  
708 prototype. It also guarantees that the present correction method will be smoothly

709 employed in predicting the dynamic response of the prototype stiffened plates by using  
710 the well-designed distorted model.

711 The present study would provide a potential approach to deal with the multi-  
712 geometric parameters distorted stiffener plate. However, it is better to reduce the  
713 number of the distorted geometric parameters (within the experimental restrictions) as  
714 small as possible to make sure a most similar dynamic response to be obtained between  
715 the distorted model and the prototype. In addition, the different mechanical parameters  
716 of plates with different thicknesses would be considered in practice test, which was not  
717 taken into account in the numerical simulations in present paper.

#### 718 **Acknowledgements**

719 *The authors acknowledge Projects supported by the Joint Foundation for Young*  
720 *Scientists of Ministry of Education (6141A02033108) and National Natural Science*  
721 *Foundation of China (11502180). The authors are also grateful for the valuable*  
722 *suggestions from Professor Magnus Langseth.*



723 Reference

- 724 1. M.A.G. Calle, M. Alves. A review-analysis on material failure modeling in ship  
725 collision. *Ocean Engineering*, 2015. **106**: p. 20-38.
- 726 2. X.S. Kong, W.G. Wu, J. Li, P. Chen, F. Liu. Experimental and numerical investigation  
727 on a multi-layer protective structure under the synergistic effect of blast and fragment  
728 loadings. *International Journal of Impact Engineering*, 2014. **65**: p. 146-162.
- 729 3. K. Micallef, A.S. Fallah, D.J. Pope, L.A. Louca. The dynamic performance of simply-  
730 supported rigid-plastic circular steel plates subjected to localised blast loading.  
731 *International Journal of Mechanical Sciences*, 2012. **65**(1): p. 177-191.
- 732 4. R.G. Teeling-Smith, G.N. Nurick. The deformation and tearing of thin circular plates  
733 subjected to impulsive loads. *International Journal of Impact Engineering*, 1991. **11**(1):  
734 p. 77-91.
- 735 5. N. Jacob, G.N. Nurick, G.S. Langdon. The effect of stand-off distance on the failure  
736 of fully clamped circular mild steel plates subjected to blast loads. *Engineering*  
737 *Structures*, 2007. **29**(10): p. 2723-2736.
- 738 6. N. Mehreganian, A. S. Fallah, L.A. Louca. Inelastic dynamic response of square  
739 membranes subjected to localised blast loading. *International Journal of Mechanical*  
740 *Sciences*, 2018. **148**: p. 578-595.
- 741 7. C. Zheng, X.-s. Kong, W.-g. Wu, F. Liu. The elastic-plastic dynamic response of  
742 stiffened plates under confined blast load. *International Journal of Impact Engineering*,  
743 2016. **95**: p. 141-153.
- 744 8. K. Micallef, A.S. Fallah, P.T. Curtis, L.A. Louca. On the dynamic plastic response of  
745 steel membranes subjected to localised blast loading. *International Journal of Impact*  
746 *Engineering*, 2016. **89**: p. 25-37.
- 747 9. J. Zhang, Q. Qin, T.J. Wang. Compressive strengths and dynamic response of  
748 corrugated metal sandwich plates with unfilled and foam-filled sinusoidal plate cores.  
749 *Acta Mechanica*, 2013. **224**(4): p. 759-775.
- 750 10. J. Zhang, R. Zhou, M. Wang, Q. Qin, Y. Ye, and T.J. Wang. Dynamic response of  
751 double-layer rectangular sandwich plates with metal foam cores subjected to blast  
752 loading. *International Journal of Impact Engineering*, 2018. **122**: p. 265-275.
- 753 11. X. Cui, L. Zhao, Z. Wang, H. Zhao, D. Fang. Dynamic response of metallic lattice  
754 sandwich structures to impulsive loading. *International Journal of Impact Engineering*,  
755 2012. **43**: p. 1-5.
- 756 12. C.P. Coutinho, A.J. Baptista, J. Dias Rodrigues. Modular approach to structural  
757 similitude. *International Journal of Mechanical Sciences*, 2018. **135**: p. 294-312.
- 758 13. A. Neuberger, S. Peles, D. Rittel. Scaling the response of circular plates subjected to  
759 large and close-range spherical explosions. Part I: Air-blast loading. *International*  
760 *Journal of Impact Engineering*, 2007. **34**(5): p. 859-873.
- 761 14. A. Neuberger, S. Peles, D. Rittel. Scaling the response of circular plates subjected to  
762 large and close-range spherical explosions. Part II: Buried charges. *International*  
763 *Journal of Impact Engineering*, 2007. **34**(5): p. 874-882.
- 764 15. X. Zhao, V. Tiwari, M.A. Sutton, X. Deng, W.L. Fourney, and U. Leiste. Scaling of the

- 765 deformation histories for clamped circular plates subjected to blast loading by buried  
766 charges. *International Journal of Impact Engineering*, 2013. **54**(0): p. 31-50.
- 767 16. L.F. Trimiño, D.S. Cronin. Non-direct similitude technique applied to the dynamic  
768 axial impact of bonded crush tubes. *International Journal of Impact Engineering*, 2014.  
769 **64**: p. 39-52.
- 770 17. M.A.G. Calle, R.E. Oshiro, M. Alves. Ship collision and grounding: Scaled  
771 experiments and numerical analysis. *International Journal of Impact Engineering*, 2017.  
772 **103**: p. 195-210.
- 773 18. R.E. Oshiro, M. Alves. Scaling of structures subject to impact loads when using a  
774 power law constitutive equation. *International Journal of Solids and Structures*, 2009.  
775 **46**(18–19): p. 3412-3421.
- 776 19. R.E. Oshiro, M. Alves. Predicting the behaviour of structures under impact loads using  
777 geometrically distorted scaled models. *Journal of the Mechanics and Physics of Solids*,  
778 2012. **60**(7): p. 1330-1349.
- 779 20. G.K. Schleyer, S.S. Hsu, M.D. White. Scaling of pulse loaded mild steel plates with  
780 different edge restraint. *International Journal of Mechanical Sciences*, 2004. **46**(9): p.  
781 1267-1287.
- 782 21. I.M. Snyman. Impulsive loading events and similarity scaling. *Engineering Structures*,  
783 2010. **32**(3): p. 886-896.
- 784 22. W. Wang, D. Zhang, F. Lu, S.-C. Wang, F. Tang. Experimental study on scaling the  
785 explosion resistance of a one-way square reinforced concrete slab under a close-in blast  
786 loading. *International Journal of Impact Engineering*, 2012. **49**(0): p. 158-164.
- 787 23. H.-M. Wen, N. Jones. Experimental investigation of the scaling laws for metal plates  
788 struck by large masses. *International Journal of Impact Engineering*, 1993. **13**(3): p.  
789 485-505.
- 790 24. F.J. Yang, M.Z. Hassan, W.J. Cantwell, N. Jones. Scaling effects in the low velocity  
791 impact response of sandwich structures. *Composite Structures*, 2013. **99**(0): p. 97-104.
- 792 25. T. Noam, M. Dolinski, D. Rittel. Scaling dynamic failure: A numerical study.  
793 *International Journal of Impact Engineering*, 2014. **69**: p. 69-79.
- 794 26. N. Jones. *Structural Impact 1997*, Cambridge: Cambridge University Press.
- 795 27. A. Morquio, J.D. Riera. Size and strain rate effects in steel structures. *Engineering*  
796 *Structures*, 2004. **26**(5): p. 669-679.
- 797 28. R.E. Oshiro, M. Alves. Scaling impacted structures. *Archive of Applied Mechanics*,  
798 2004. **74**(1-2): p. 130-145.
- 799 29. R.E. Oshiro, M. Alves. Scaling of cylindrical shells under axial impact. *International*  
800 *Journal of Impact Engineering*, 2007. **34**(1): p. 89-103.
- 801 30. L.M. Mazzariol, R.E. Oshiro, M. Alves. A method to represent impacted structures  
802 using scaled models made of different materials. *International Journal of Impact*  
803 *Engineering*, 2016. **90**: p. 81-94.
- 804 31. Z. Luo, Y. Zhu, X. Zhao, D. Wang. Determination method of dynamic distorted scaling  
805 laws and applicable structure size intervals of a rotating thin-wall short cylindrical shell.  
806 *Proceedings of the Institution of Mechanical Engineers, Part C: Journal of Mechanical*  
807 *Engineering Science*, 2015. **229**(5): p. 806-817.
- 808 32. Z. Luo, Y.P. Zhu, X.Y. Zhao, D.Y. Wang. High-Order Vibrations' Dynamic Scaling

- 809           Laws of Distorted Scaled Models of Thin-Walled Short Cylindrical Shells. *Mechanics*  
810           Based Design of Structures and Machines, 2015. **43**(4): p. 514-534.
- 811   33.    U. Cho, A.J. Dutson, K.L. Wood, R.H. Crawford. An advanced method to correlate  
812           scale models with distorted configurations. *Journal of Mechanical Design*, 2005.  
813           **127**(1): p. 78-85.
- 814   34.    S. Yao, D. Zhang, F. Lu, X. Chen, P. Zhao. A combined experimental and numerical  
815           investigation on the scaling laws for steel box structures subjected to internal blast  
816           loading. *International Journal of Impact Engineering*, 2017. **102**: p. 36-46.
- 817   35.    X. Kong, X. Li, C. Zheng, F. Liu, W.-g. Wu. Similarity considerations for scale-down  
818           model versus prototype on impact response of plates under blast loads. *International*  
819           *Journal of Impact Engineering*, 2017. **101**: p. 32-41.
- 820   36.    C. Zheng, X.S. Kong, W.G. Wu, S.X. Xu, Z.W. Guan. Experimental and numerical  
821           studies on the dynamic response of steel plates subjected to confined blast loading.  
822           *International Journal of Impact Engineering*, 2018. **113**: p. 144-160.
- 823   37.    W.E. Baker. *Explosions in Air 1973*, Austin and London: University of Texas Press.  
824           150-167.
- 825   38.    G.S. Langdon, A. Ozinsky, S. Chung Kim Yuen. The response of partially confined  
826           right circular stainless steel cylinders to internal air-blast loading. *International Journal*  
827           *of Impact Engineering*, 2014. **73**: p. 1-14.
- 828   39.    AUTODYN library, in *Century dynamics incorporated. USA:2007*.
- 829   40.    Z. Zhang, C. Xiao, L. Chen, C. Wang, Y. Huang. Approximate scaling method of  
830           stiffened plate subjected to underwater explosion blast. *Journal of Ship Mechanics*,  
831           2010. **14**(11): p. 1276-1283.